AIAA SciTech Forum
7-11 January 2019, San Diego, California
AIAA Scitech 2019 Forum

10.2514/6.2019-0198

Detonation Wave Dynamics in a Rotating Detonation Engine

Fabian Chacon*, and Mirko Gamba†
University of Michigan, Ann Arbor, MI 48109

Rotating detonation engines have complex unsteady flow fields that have been observed to give rise to multiple wave systems beyond the main detonation wave they are intended to produce. In this work we have developed a new analysis technique we refer to Circuit Wave Analysis to identify and describe the system of waves associated with the reaction fronts that exist in the RDE from time-resolved, high-speed end-view chemiluminescence movies of the reaction fronts. For each wave system, we then extract the speed of the wave, its direction and strength (from a measure of spectral power). Through this approach we have determined that under a range of operating conditions RDE flow fields are characterized by three separate wave systems: the main detonation wave and two secondary wave systems, which, based on their relationship relative to the main detonation wave, we refer to as the counter rotating fast wave and counter rotating slow wave pair, respectively. The properties of all three waves vary with both operation condition (air mass flow rate and equivalence ratio) and the configuration of the air inlet and fuel injector. The controlling mechanisms behind the secondary wave systems are not currently known. However, the impact that secondary waves have on some of the detonation properties can be observed in select cases. For example, the presence of a secondary wave has been observed to correspond with a reduction in detonation wave speed.

I. Introduction

RDEs are a type of combustor that use detonation waves to consume reactants instead of deflagration waves as in traditional gas turbine engines. The use of detonation over deflagration causes a pressure rise during combustion, an effect that is termed pressure gain combustion. This pressure gain allows for additional work to be extracted by the turbomachinery, thus increasing the thermal efficiency of the cycle.

A RDE is composed of an annular channel with a width that is small compared to the diameter of the device. Fresh reactants are continuously fed into the device in the axial direction by an injection system; injection of fuel and oxidizer is typically separate (non-premixed). A detonation wave travels within the channel in the azimuthal direction consuming the fresh reactants along the entrance to the channel; post-detonation gases are then exhausted at the opposite end of the channel.

Because the detonation waves present in RDEs travel at very high speeds on the order of 1 to 2 km/s,[1–4] the use of high-speed measurement instrumentation is required. Therefore, for test times lasting a few seconds large amounts of data are generated recording thousands of operation cycles. In this work we analyze chemiluminescence video acquired in a laboratory scale RDE in order to characterize the prevalence (whether a given wave system is present) and velocities of secondary wave systems under different conditions of operation (mass flow rates and global equivalence ratios). Secondary wave systems have been observed by a number of experimental groups for a variety of injection schemes and operation conditions.[5–7] Previous work has shown it is possible to extract detonation wave speed information from x-t diagrams using image analysis techniques such as the Hough transform. Here we will present a technique capable of identifying any number of wave systems in a systematic manner.

In this study we detail a new method for the identification of waves traveling in closed circuits we term Circuit Wave Analysis. This technique is composed of a series of mathematical operations that together

*Graduate Student Research Assistant, Dept. of Aerospace Engineering.
†Associate Professor, Dept. of Aerospace Engineering.

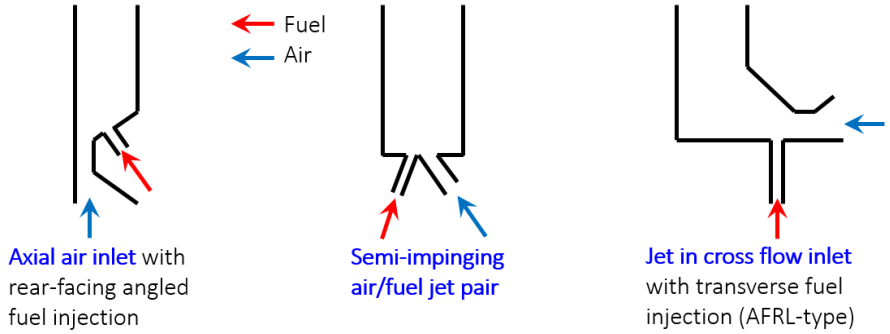

Figure 1. Stylized depictions of the three air inlet / fuel injection configurations considered in this study.

allow for the identification of multiple wave systems in RDEs. Through the use of the technique we are able to assess quantities such as wave speed, direction, strength (a measure of spectral power), and wavelength. We have found that across the three injection schemes we have investigated there are three independent wave systems that may appear during detonation operation. These three wave systems have been termed, the detonation wave, the counter propagating fast wave, and the counter propagating wave pair. The speed, prevalence, and strength of the two secondary wave systems varies throughout the operation regime, depending on air mass flow rate, equivalence ratio and injector scheme. While the origin of these waves is currently under investigation, some of the potential impacts they may have are discussed. In particular the counter propagating wave pair is correlated with a reduction in detonation wave speed. This observation is consistent with additional work at the University of Michigan investigating parasitic combustion in RDE flow fields.[8,9]

II. Description of the Experimental Setup

In this section we will briefly describe the experimental setup, including the overall geometry of the RDE, injection schemes, instrumentation, as well as the control scheme used to capture all data. Additional information can be found in a previous study on the same hardware and data sets in Duvall et al.[10]

A. Description of the RDE and Air/Fuel Handling Systems

The MRDE is a six inch outer diameter laboratory scale RDE. It is composed of a series of stackable elements that define the body of the RDE and the internal flow path, which is defined by properly contoured interchangeable plates. This overall design allows for implementing and testing a variety of air inlet and fuel injector configurations solely by replacing one or two plates. The tree air inlet / fuel injection configurations shown in figure 1 are considered in this work and correspond to canonical configurations that could be found in RDEs for different applications. The first configuration is an axial air inlet with discrete fuel injector and it is a configuration that could be intended for jet engine applications with axial turbomachinery.[11] The second configuration is a semi impinging doublet jet injector and could be found in rocket applications.[12] The third configuration is a radial air inlet with transverse fuel injection (jet in crossflow type), which is perhaps the most widely studied configuration[7] and is applicable for engines relying on centrifugal compressors such as those intended for helicopters.

1. Axial Air Inlet Injector

The axial air inlet (AAI) configuration is based on a geometry that was considered in a computational work conducted at the Naval Research Lab.[11] The air inlet flow consists of air flowing axially over a smooth one-sided contoured surface. This surface narrows down to a injection gap of 1.52 mm around the entire channel, for an area ratio between the channel and the throat of 5:1. Fuel is injected into the detonation channel from the upper face of the contour from 120 evenly spaced individual jets with a diameter of 0.89

mm arranged around the circumference of the contour. The jets are perpendicular to the face of the contour which is itself angled at 30 degrees below the horizontal toward the outer wall of the MRDE.

2. Semi-Impinging Jet Injector

The design for the semi-impinging jet (SIJ) configuration is based on a geometry that was considered in a computational work done at ONERA.[12] The design utilizes staggered jets arranged around the circumference of the detonation channel. The jets are angled toward the center of the channel with oxidizer injecting from the inner radius and fuel from the outer radius. A key feature of the injectors is that the fuel and oxidizer jets are offset in such a way that the jets only overlap over a fraction of their exit area. In this design the injectors are oriented such that they inject towards the middle of the channel, unlike the ONERA scheme where they inject azimuthally. This change over their design was needed to facilitate machining considerations. The injectors consist of 120 evenly spaced holes with a diameter of 0.89 mm for fuel, and 1.2 mm for air.

3. Jet in Crossflow Configuration (AFRL)

The jet in crossflow (JIC) configuration is a radial air inlet with transverse fuel injection and it is based on the RDE operated by the Air Force Research Lab at Wright Patterson Air Force Base.[7] In this scheme air flows radially around a chamfered corner expanding radially from an inner plenum. As the air flow goes around the corner it entrains fuel from transverse injectors that are oriented axially. The fuel injectors consist of 120 evenly spaced holes with a diameter of 0.89 mm. This design was included because of its extensive use in computational and experimental research in the field, as well as the simplicity of the configuration. As such it serves as a benchmark to which other configurations can be compared.

B. Instrumentation and Measurements

The outer wall and the (air/fuel) plenum chambers of the RDE are instrumented with various piece of instrumentation. A summary of the outer-wall instrumentation is give in figure 2 where the outer wall is unwrapped to show the distribution of the instrumentation. In addition, optical access to the detonation chamber is available from the exhaust side, and it is used to collect high-speed chemiluminescence videos of the detonation wave propagating through the detonation channel.

The outer wall is instrumented with 16 capillary tube average pressure (CTAP) measurements points. CTAPs are constructed from 1 mm diameter, 90 cm long flush-mounted capillary tubes terminated with a slow response pressure transducer. The CTAPs are distributed axially at a fixed azimuthal location as shown in figure 2. They span from upstream of the air slot contraction to the mid-length point to the detonation chamber. One more CTAP measurement point is located near the open end of the detonation channel. The outer wall is also instrumented with four high-speed pressure transducers. Two transducers are flush-mounted Kulite transducers and are located axially at a fixed azimuthal location as indicated in figure 2. Finally, two transducers (PCB 113B26) are recess mounted and are located at a fixed axial location and separated 45° apart straddling the azimuthal location of CTAP measurements. A microphone (PCB) located in the test room approximately two meters away from the device is used to record the acoustic signature of the operation conditions, and it is used to monitor the operation of the device.

High-frame rate chemiluminescence video of the detonation wave as observed from the exhaust of the RDE were taken with a high-speed CMOS camera (Phantom v711) operating at 55,016 frames per second with an exposure time of 10 μs. The camera uses a 50 mm lens to acquire a field of view of about 174 mm $\times$ 169 mm with a resolution of 288 $\times$ 280 pixels. The camera observed the exit of the RDE axially into the device through a fused quartz window built into the exhaust system from approximately two meters away.

C. Control and Data Acquisition Systems

The test facility utilizes a high-pressure air and fuel supply systems, and a high-temperature exhaust. Electro-pneumatic solenoid ball valves and precision orifices are used to control and meter the flow of reactants to the MRDE. Pressure controllers are used in conjunction with air loaded regulators to set the fuel and air pressures. Cold flow testing is performed beforehand with pressure measurements taken across the orifices to verify choked flow by comparison with the critical pressure ratio. Control of all hardware and operation of the device is conducted with a LabVIEW-based controller. The timing sequence during a run is directly controlled by a LabVIEW controller with dedicated data acquisition cards (NI PCI-6259). All high speed

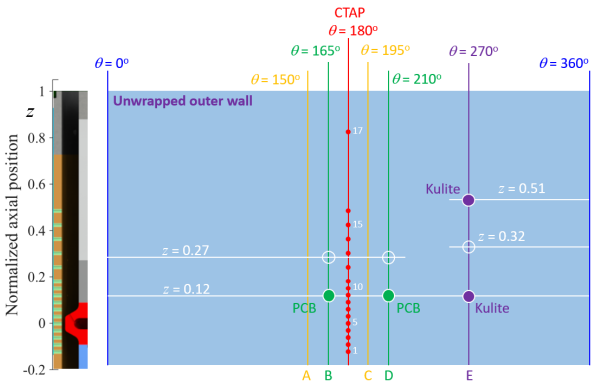

Figure 2. Schematic diagram showing the azimuthal and axial location of various sensors on the outer wall of the RDE.

measurements are taken with an additional dedicated LabVIEW data acquisition card (NI PCI-6133). The MRDE is directly connected to an exhaust system, and uses a downstream afterburner as the ignition source.

III. Circuit Wave Analysis

One of the key challenges in understanding the wave dynamics of RDEs is the need to systematically capture information about any waves travelling in the annulus that contribute to the overall dynamics of the system. Of particular interest is the existence and impact of waves secondary to the primary detonation wave(s). Hence, the speed, direction, wavelength, amplitude information of these waves and how they interact with each other is of interest. In previous work, some information about wave dynamics have been extracted from detonation chamber pressure measurements such as peak pressures, here we follow the same approach for estimating these quantities.[13] In this study we extract detailed information about the system of waves that may exist during operation of the RDE from the high-speed movies of chemiluminescence collected at the open end of the RDE. Before discussing the results in the next section, in this section we discuss an analysis technique, which we refer to as *circuit wave analysis*, that we have developed to analyze high-speed chemiluminescence videos to identify any wave system present during operation and extract their properties of interest. The techniques is based on a sequential application of a series of operations that once combined, allow us to extract the desired information. Circuit wave analysis is based on the following operations: (1) construction of the x-t diagram from end-view, high-speed videos of chemiluminescence; (2) application of a Galilean shifted Fourier transform to the resulting x-t diagram, from which wavelength and strength are extracted; and (3) application of the modified Radon transform to extract speed of any wave that exist during the operation of the device. This technique is called wave circuit analysis because, while we have developed it for use in RDE research, it is applicable to any system with periodic boundary conditions (what we call a closed circuit) and with information available throughout the circuit. In our case the circuit is composed of the detonation annulus for which we have high framing rate chemiluminescence videos for the entire annulus.

A. Construction of the x-t Diagram

The high speed chemiluminescence video of the annulus was processed into a space-time diagram (here simply referred to as x-t diagram) for a portion of the steady flow. The technique used to construct x-t diagrams is similar to the technique used at the Air Force Research Lab.[14] For each frame of the video the annulus is discretized into 101 sectors distributed evenly over the azimuthal dimension of the annulus and the light intensity within each sector is integrated and normalized by the number of pixels into a single value for each sector for each frame. In practice, this reduces each image in the video to a column vector of light intensity. Combining all of the frames throughout the video creates a matrix, or the x-t diagram, showing the propagation of the waves (i.e., the trajectory) through the device. An example x-t diagram constructed for a representative case of operation of the MRDE is shown in figure 3 where the x-axis is time and the

y-axis is the angular position in the channel.

B. Galilean Shifted Fourier Spectrum

The Galilean Shifted Fourier Spectrum (GSFS) is an analysis step that we have developed by combining a Galilean shift to a time-resolved signal with its Fourier transform to readily identify the existence of the coherent propagation of features that we generally term as "waves". This approach facilitates the determination of various properties of the waves traveling through the annulus of the MRDE. This technique is applied to the x-t diagram constructed from the high-speed chemiluminescence and identifies the following information: (1) wave speed, (2) wave direction, (3) wave temporal frequency, and (4) wavelength. Additional processing of the GSFS also allows for the formulation of a measure of spectral power we call strength.

The basic principle of the technique is to use the lab reference frame x-t diagram to construct a second "velocity shifted" x-t diagram that would have been observed had the observer (i.e., the camera) been spinning at a fixed angular velocity Ω (magnitude and direction). In practice, this is a Galilean frame of reference shift to the whole x-t diagram. Upon construction of the shifted x-t diagram, a one-dimensional temporal Fourier transform is taken for all location in the annulus (i.e., along each row of the x-t diagram). We then repeat the process for a range of angular shift velocities Ω and organize the results in a shift velocity vs frequency plot. It is the combination of these shifted Fourier transforms over a range of shift velocities that results in what we term the Galilean Shifted Fourier Spectrum. The usefulness of the technique lies in the observation that at the correct angular shift velocity the detonation wave will appear stationary and the frequency associated with it will fall to zero. This is true of any wave regardless of direction or speed, so long as it is approximately periodic for the duration of time considered. We can then apply this method to the full x-t diagram to extract time-average wave properties, or to a short section of the x-t diagram (e.g., for a time duration equivalent to N_c cycles, such as $N_c = 10$) to evaluate the temporal variation of the wave properties during the operation of the device.

Let $\mathbf{D}$ denote the x-t diagram made of an $N \times M$ matrix, where N (subscript i) is the number of discretized bins distributed over the annulus and M (subscript j) is the number of snapshots. Then each row of the GSFS can be expressed as follows:

$$G_{k,p} = \max\{\mathscr{F}(D_{i,*;k})\} = \max\{\hat{D}_{i,p}\} \tag{1}$$

for $i = 1, ...N$ and collectively define the GSFS matrix $\mathbf{G}_k$ at a specific shift velocity v_k. The quantity $\mathscr{F}(D_{i,*;k})$ denotes the one-dimensional Fourier transform along the i-th row of a Galilean shifted x-t diagram $\mathbf{D}_k$ resulting in frequencies f_p, which is expressed as

$$D_{i,j;k} = D_{l,j} \tag{2}$$

for $j = 1, ...M$, and where l is a linear interpolation of azimuthal position and light intensity within a time column based on the following definition, with periodic bounds on l:

$$l = (x_0)_i + v_k t_j \tag{3}$$

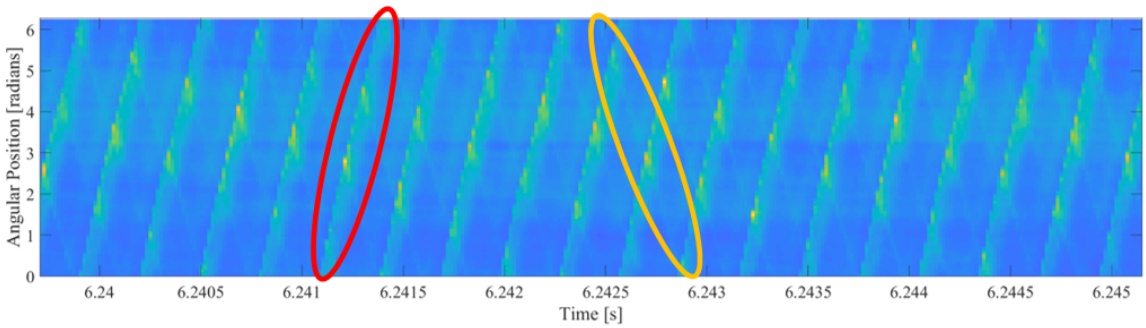

Figure 3. Example x-t diagram made from high speed chemiluminescence for a representative run of the MRDE, showing waves traveling in the positive azimuthal direction. The main detonation wave is shown circled in red, while one of the counter propagating wave pair is circled in yellow.

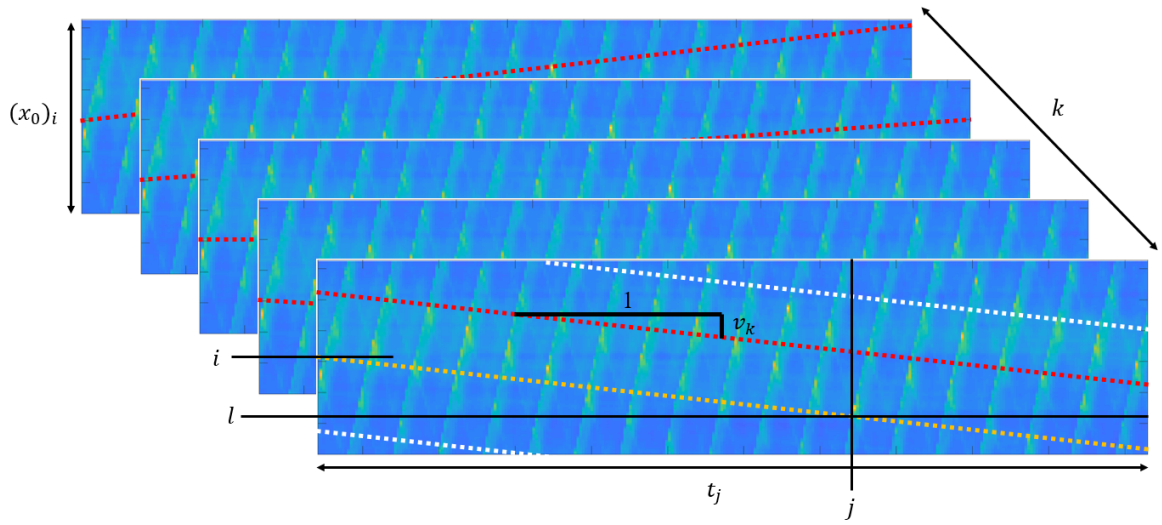

Figure 4. Visualization of the process to construct a GSFS from the initial x-t diagram constructed from high speed video. Different azimuthal bins will have different spectra, all bins must be considered. For simplicity three bins are shown in red, yellow, and white, along with their corresponding trajectories in time and space.

Here $v_k = \Omega_k R$ is the shift velocity (it has a magnitude and direction defined by its sign) associated with angular shift velocity Ω_k for a circuit of radius R, t_j is the time associated with the column being shifted, and $(x_0)_i$ is the initial azimuthal position of a given row. The equation is used to find the Galilean shifted position for each snapshot in time. Here v_k can take on any value and to construct a GSFS it is necessary to apply a shift velocity over a range of values (magnitude and direction). When $v_k = 0$ it is equivalent to taking the Fourier transform of the lab reference frame x-t diagram. The entire mathematical process can be visualized as shown in the example of figure 4.

By shifting over a range of velocities it is possible to identify the presence of a wave, its speed and its direction. When the shifted velocity v_k matches the wave speed and direction, the observed rotational frequency of that wave will be reduced to zero. It is important to note that for every reference frame and resulting x-t diagram, each row of the x-t diagram will result in a unique temporal Fourier spectra. In order to reduce these many spectra to one it is possible to take an average where:

$$G_{k,p} = \frac{1}{N} \sum_{i=1}^{N} \hat{D}_{i,p} \tag{4}$$

where p denotes the index of the frequency resulting from the Fourier transform. However instead we take the maximum value for a given frequency f_p across all N observers, or simply:

$$G_{k,p} = \max\{\hat{D}_{i,p}\} \tag{5}$$

This is because a wave becomes stationary in its reference frame. In this reference frame a set of observers (i.e., azimuthal bins) along the circuit do not all see the same light intensity. An observer at the detonation wave for instance will see a higher intensity than one ahead of it in the fill region. However, in the lab reference frame all observers along the circuit see a wave of approximately equal intensity passing by at the rotational frequency of the wave. In order to preserve the spectral power when a wave becomes approximately stationary, the maximum is taken rather than an average. The process outlined above results in diagrams that can be used to identify the various properties of all waves present in a closed circuit system.

An example of a representative GSFS plot constructed for a reference case of typical RDE operation is shown in figure 5. From this GSFS it is possible to identify important features. For instance the grouping of straight lines emanating from the $a_k/D_{CJ} = -0.8$ y-intercept indicate a grouping of harmonics all of which travel at the same speed ($0.8D_{CJ}$) in the clock-wise azimuthal direction (negative value) within the annulus. In addition, the different slope of each straight line in this grouping each indicate a different wavelength corresponding to separate harmonics, with the line of largest slope representing the fundamental. The slope

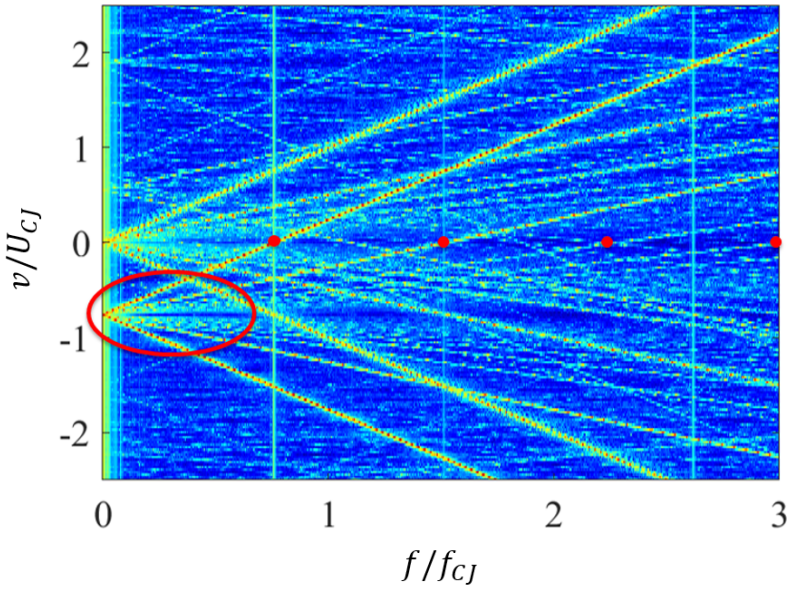

Figure 5. Example GSFS showing the main propagation direction of the detonation wave as well as secondary waves present in the system. The y-intercept of the main detonation wave is highlighted by the red circle. Harmonics of the wave in the zero velocity shifted frame of reference are indicated with red dots.

of the line corresponding to the fundamental represents the wavenumber of that wave, which once combined with its propagation speed allows to determine the number of waves. This analysis technique produces information similar to a 2-D Fourier transform over space and time directly applied to the x-t diagram, but this representation allows for easier identification of coherent wave structures such, as the detonation wave and secondary waves, which are mathematically represented by a series of waves all moving at the same velocity.

When in a wave speed reference frame all frequencies associated with a wave tend toward zero, the spectral power of a given wave is fixed regardless of the reference frame. In the wave reference frame it is then possible to integrate over a small range of low frequencies to get the total spectral power associated with the wave (including all of its harmonics) without any contribution from other waves. We refer to the total spectral power associated with a wave as *strength*, and it is used to quantify the relative power associated with a wave. Integration is most easily achieved once velocity information has been extracted from the GSFS, which is the next step in the analysis method. The representation of the wave system captured by the GSFS lend itself to conveniently and automatically identify the wave speed and number using a modified Radon transform operation, which is the last step of the processing. Note that more than one wave system can be captured by the GSFS, where each wave system is represented by a grouping of lines with properties similar to the one described here and shown in the example of figure 5. In fact, as we will discuss further below, this method allows us to identify secondary and tertiary waves in addition to the primary detonation wave.

C. Modified Radon Transform

While the GSFS is very intuitive for the identification of waves to the naked eye it still needs to be further processed to extract wave speeds and directions in an automated fashion. In order to do this we can reduce the GSFS to a series of curves that are easier to manipulate automatically through a modified Radon transform. The Radon transform is a method typically used in image processing for identifying lines in images and is a more general transformation of the Hough transform. A line can be constructed using two parameters, the angle the perpendicular of the line makes with the a reference axis (e.g., the x-axis), θ, and the minimum distance between the origin of the coordinate axis and the line, r. This transform allows to project a single pixel in real space of the image onto a curve in $r-\theta$ space describing all possible lines that pass through that pixel. If two pixels lie together on a line then the two curves in $r-\theta$ space overlap. We then superimpose the

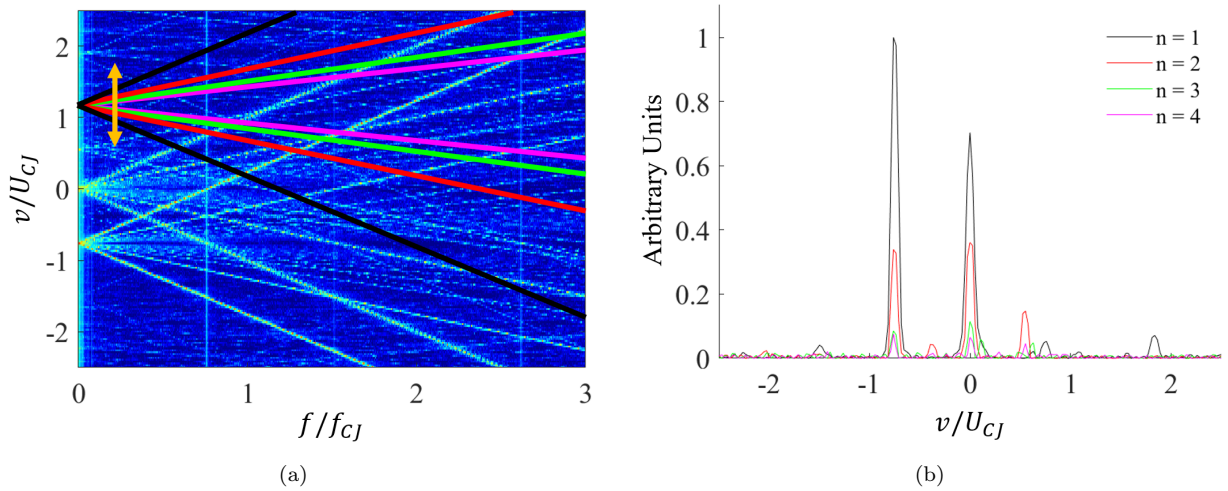

(a) (b)

Figure 6. Visualization of the modified Radon transform principle used to construct curves identifying the presence of various waves at a variety of speeds. Part a) shows an example GSFS with the first four wave number 'V' shapes being swept along the velocity axis, and part b) shows the resulting modified Radon curves.

value of each transform over any number of curves that intersect. This creates a contour map in $r-\theta$ space. Large peaks in the transformed space correspond to bright lines in the original space with the coordinates of the peak giving both defining parameters of the line. This basic idea can be modified to look for any arbitrary shape in images that can be properly parameterized.

In the case of the GSFS the shape we are interested in is the characteristic sideways 'V' shape made by waves in the circuit. Because the waves we are interested in take place in a closed circuit with periodic boundary conditions, waves can only have an integer number of waves in the circumference. This means that the wavelength of a given wave is either C, $C/2$, $C/3$, ... etc. where C is the circumference of the closed circuit. Because they are discrete values so too are the slopes. Because the slopes are discrete values and always emanate from the zero frequency axis, we can parameterize the 'V' shape as being based solely on wave speed and the wave number. In order to compute the transform for a given wave number, it is only necessary to sum pixel values which lie along a pair of lines that correspond to the 'V' shape. In our case we have normalized both velocity and frequency by the ideal detonation speed, this causes waves with a wavelength of 1 (i.e., one wave in the annulus) to appear as lines with slopes of 1 and -1, wavelengths of 1/2 have lines with slopes of 1/2 and -1/2 etc. This allows for the easy construction of the target shape as a pair of lines intersecting on the y axis with slopes corresponding to the wavelength of the wave.

The technique amounts to a sliding filter applied to the GSFS, where pixel values underneath the filter window are summed. When the filter lies over a region without a wave as shown in figure 6(a) the integrated values will be low, whereas when it crosses over the region corresponding to the detonation all four wave shapes will register large values when integrated. Each wave shape is swept independently resulting in peaks for some wave numbers that are unique and do not appear in other wave numbers. In figure 6(a) the first four wave number shapes are shown being swept along the speed axis, with the resulting curves being shown in figure 6(b). By turning the GSFS into a set of curves the process of extracting wave speeds becomes relatively simple, and lends itself readily to automation. Quadratic curve fitting can then be used for peak finding to estimate wave velocity with sub-resolution accuracy. Once the wave velocities are known, additional information can be extracted from GSFS, particularly the strength of the wave.

D. Properties and Benefits

Circuit wave analysis (CWA) has a number of benefits over various other analysis techniques that have been used in the literature. Circuit wave analysis is capable of identifying any number of wave systems present in the annulus of an RDE even those that are very weak (in intensity) compared to the detonation wave, a current limitation of line identification algorithm approaches. However, it does not have as good a temporal resolution as the line algorithm approaches. The use of the GSFS does allow for improved temporal capabilities when compared to 2D spatio-temporal Fourier transforms. This is because the modified Radon

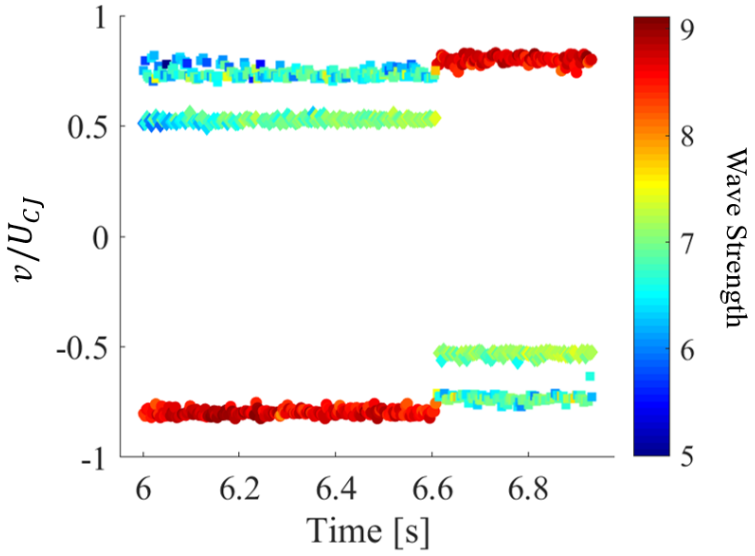

Figure 7. Example of temporally resolved application of CWA. Information about three wave systems detected by the method are shown. Circles refer to the main detonation wave, squares to a counter propagating fast wave, and diamonds to a counter propagating slow wave pair.

transform looks for shapes in the GSFS that depend on speed rather than frequency, thus it is insensitive to the reduction of frequency resolution needed to gain temporal resolution. This allows the use of CWA over short periods of time while still being able to accurately measure wave speed. An example of such a computation for one of our runs is shown in figure 7, where CWA is performed over an interval of time equivalent to 7 detonation cycles for the entire duration of the run, allowing to describe the temporal variation of wave speed, wave strength, and direction for three wave systems that exist in the operation of RDE under the specific conditions of this case, the nature of the three waves will be exapanded upon in the next section. In figure 7 three sets of data are shown and differentiated by symbols shape. Each set of data refers to a different type of wave, which all co-exist in the operation configuration of the case of figure 7. The figure shows the time variation of the speed of each of the three waves (normalized by the ideal detonation wave speed at the nominal global equivalence ratio). The color of the symbols is used to indicate a measure of the strength of a given wave at a given time. They are shown on a logarithmic scale due to the large dynamic range between the main detonation wave and the far dimmer secondary waves.

IV. Investigation of Secondary Wave Systems by the Application of CWA

From the Circuit Wave Analysis(CWA) outlined above we have identified three dominant wave systems existing in the annulus for all of our injector configurations and across the operating conditions when the system operates in detonation mode. The relative strength and prevalence of any of the wave systems depends on the configuration of the air inlet and fuel injection schemes being used as well as the operating conditions (mass flow rate and equivalence ratio). The three waves that we have identified and we describe further are:

1. The main detonation wave that propagates with speed D;
2. A fast wave traveling counter to the primary detonation wave (or simply a counter propagating fast wave) at approximately the same speed of the primary detonation wave, or generally at a speed U_F;
3. A slow moving pair of co-rotating waves spaced 180^o apart that move counter to the primary detonation wave (or simply a counter propagating slow wave pair) at a speed U_P.

The three waves described here do not account for all of the tones and waves that might be identified in the spectra constructed from high-speed pressure measurements and chemiluminescence videos.[10,13] They are

however the three wave systems for which the data suggests physical independence. Here we mean physical independence to mean that they are physical processes occurring in the device rather than a mathematical artifact describing the physics of one of the waves or the interaction between different waves. This conclusion was made because all three waves are identifiable in all measurements taken thus far, including direct observation in x-t diagrams without any processing techniques beyond the x-t diagram. Tones and waves not described in this section are currently believed to be the result of the Fourier representation describing non-linear processes or interactions between the three waves described here. This is an aspect that we are further evaluating.

The presence of these three waves is determined with CWA. However, to remove waves that are considered weak, a lower cutoff value for the intensity of light associated with one of the two secondary wave systems was placed at 150 times dimmer than the main detonation wave. In the next section we describe the properties of each of the three wave systems further.

1. Detonation Wave

The primary detonation wave has been observed in all of our injection geometries to travel at approximately 0.75 to 0.85 D_{CJ}. This was initially observed in high-speed pressure measurements and high-speed chemiluminescence videos. Through the use of the GSFS, what were previously thought to be harmonics can now be confirmed. In figure 5 it can be seen that all harmonics of the detonation wave emanate from the same velocity shift intercept, circled in red. These waves emanating from this intercept move with the same velocity as one another and correspond to the harmonics of the detonation wave. In the stationary frame of reference shown by the zero shift velocity line, these tones become 0.8 and its harmonics.

2. Counter Propagating Fast Wave

For all injectors, a counter propagating wave moving at approximately the same speed or moderately slower (up to 200 m/s) than the main detonation wave but counter to it was detected for some operation conditions. This secondary wave is difficult to detect with a single pressure sensor because when its speed matches the detonation wave speed they cannot be differentiated from it. It is however readily identified through CWA. For most conditions this counter propagating wave is much dimmer than the main detonation wave, typically 1 to 2 orders of magnitude. It is most apparent in the SIJ injector, here the fast counter propagating wave approaches both the same speed and spectral power as the primary detonation wave.

3. Counter Propagating Slow Wave Pair

For all injection schemes, certain operations conditions result in a tertiary tone not associated with a detonation. This tone presents itself in high-speed pressure measurements as spectral content at approximately $1.05 f_{CJ}$. CWA shows that this tone corresponds to a pair of waves co-rotating counter to the propagation of the main detonation wave at a velocity of approximately $0.5 D_{CJ}$ or 1000 m/s, which correspond approximately to the acoustic speed of the post-detonation gases. These waves can also be observed directly in the x-t diagram shown in figure 3 circled in yellow. Thes spectral power of thsee counter propagating waves are typically an order of magnitude weaker than the that of the detonation wave.

V. Prevalence of Secondary Wave Systems

Information extracted with the use of CWA allows for the construction of more detailed operation maps. Previous operation maps for the MRDE could only identify whether the engine operated in the detonation mode or not, the detonation mode being characterized by any number of detonation waves. These maps are shown in figures 8(a) through 8(c). For most operating conditions we have tested we observe detonation being successfully stabilized in the annulus of the RDE within a fraction of a second and persisting until the end of the experimental run. The exceptions for the AAI are at low air mass flow rates and high equivalence ratios. For the JIC configuration, low equivalence ratio operation results in (longitudinal) pulsed combustion.

With CWA results we are able to construct what we term wave maps for operation conditions that result in detonation. These wave maps are shown in figures 8(d) through 8(f) and show whether a given secondary wave is present in the MRDE for a given injector configuration and operating condition. We term prevalence the existence of any of the three wave systems.

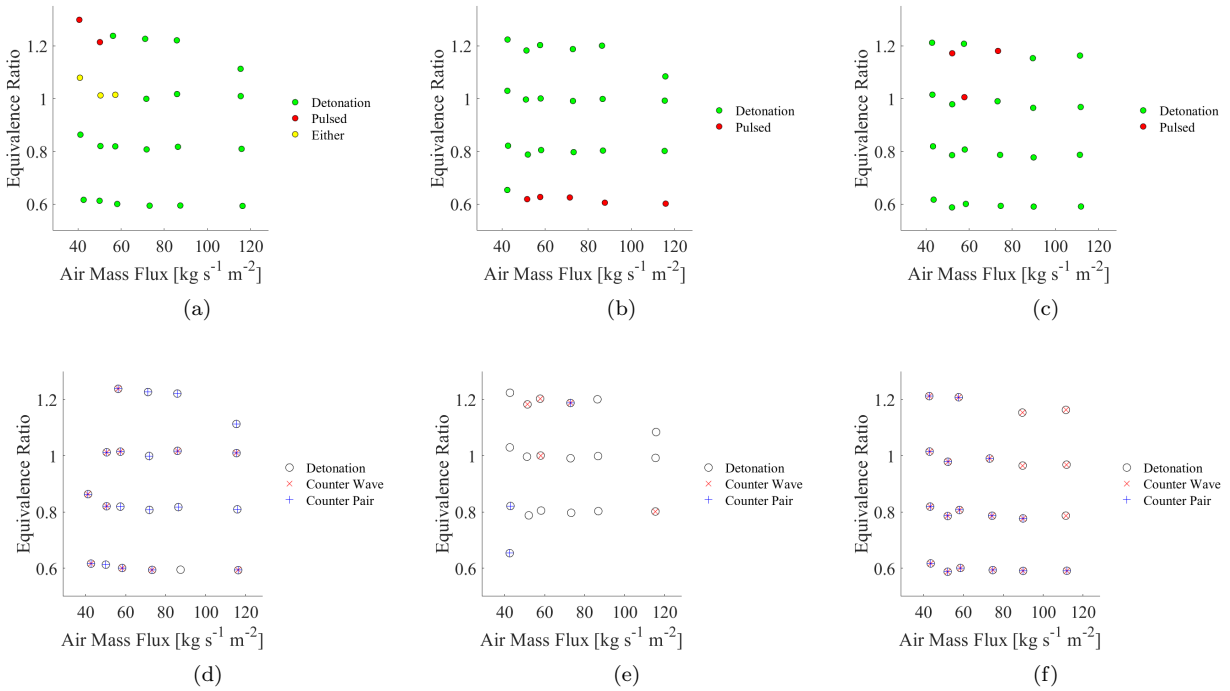

Figure 8. a)-c) operation maps for the three injection configurations showing the operation mode for given operation conditions. d)-f) shows the prevalence of secondary waves for the same conditions of a)-c). Case a) and d) correspond to the AAI configuration; case b) and e) correspond to the JIC configuration; and c) and f) correspond to the SIJ configuration.

For the AAI and JIC configurations there is no easily discernible trend in the prevalence of a given wave. However for the SIJ injector the counter propagating slow wave pair ceases to exist at higher equivalence ratio and air mass fluxes. This corresponds to regions of increasing fuel mass flow rate. Because the mechanisms that sustain and drive the secondary wave systems are not currently known, it is difficult to hypothesize as to why this may be the case. Understanding the nature and source of these waves is the focus of current work. It should be noted that both operation maps and wave maps were constructed during steady operation, during which mass flow rates, spectral content, and detonation wave propagation direction, were either held or observed to be constant.

VI. Speed of Secondary Wave Systems

As part of our initial investigation into the wave dynamics of RDEs we have compiled the mean speeds for all three wave systems across all injectors for all cases that result in detonation. Here we have plotted them together in a set of plots in figure 9. Each plot compares one of the three wave speeds against one of the other two, with all speeds having been normalized. The detonation wave and the counter propagating fast wave are normalized by the ideal detonation velocity D_{CJ} ($\approx$1900 m/s) and the counter propagating wave slow pair by the ideal detonation products speed of sound a_{CJ} ($\approx$1000 m/s) evaluated at the nominal global equivalence ratio of that particular operating point. It is important to note that points in a given plot are only shown if that operation condition resulted in both waves being compared. Values for the detonation speeds are denoted with the subscript D, the counter propagating fast wave with subscript F, and the counter propagating slow wave pair as subscript P. Across all cases the detonation speed ranges from 0.6 to 0.9 of D_{CJ}, with the counter propagating fast wave having a similar range of values. The counter propagating slow wave pair is slower, traveling in the range 0.9 to 1.1 of a_{CJ}. The counter propagating wave pair speed is very near the sonic speed of detonation products in all cases, suggesting the wave is closely related to acoustic modes of the annular combustion chamber. The most immediate trend seen in the speed data is in figure 9(a). Here the majority of points lie on the diagonal line denoted by a red dashed line. The strong relationship between the two speeds suggest that the propagation of the two waves is inherently

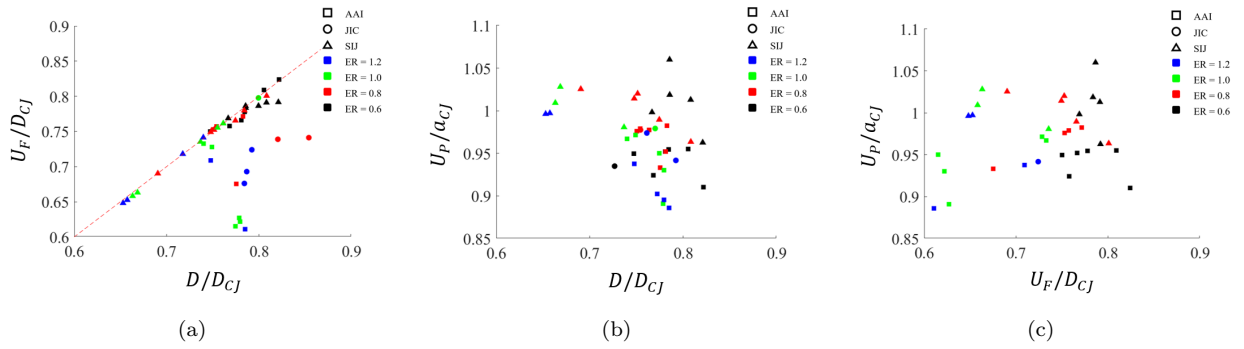

(a) (b) (c)

Figure 9. Summary of the speed of each of wave system across all operating conditions: a) Counter propagating fast wave speed as a function of detonation speed; b) Counter propagating slow wave pair speed as a function of detonation speed; and c) Counter propagating slow wave pair speed as a function of counter propagating fast wave speed.

coupled. This is not always the case as evidenced by those points that lie off the diagonal line. The reason for a given operation condition resulting in one behavior versus the other is not currently known. All air inlet and fuel injector configurations have exhibited both behaviors depending on operation condition. In figure 9(b) there is a possible equivalence ratio dependence on the relationship between the main detonation speed and its counter propagating slow wave pair. For a given equivalence ratio there is a reciprocal trend between the two quantities. With higher detonation speeds being associated with lower wave pair speeds. Higher equivalence ratios tend to move the curve closer to zero while lower equivalence ratios push the curve further out. Currently there is no readily discernible trend in figure 9(c). Understanding the driving mechanics behind these velocities is the focus of current work.

VII. Potential Secondary Wave Effects

While the source and propagation mechanisms of the secondary wave systems are not currently understood, some of the potential effects they have on RDE operation and performance can be observed in select cases. In a set of data taken during long duration experimental runs on the AAI configuration, the counter propagating slow wave pair was observed to disappear after approximately two seconds of run time. During the entire run flow rates were kept stable to the same nominal condition of 90 $kg\ s^{-1}\ m^{-2}$ with an equivalence ratio of 0.6. Upon the disappearance of the secondary wave, the speed of the main detonation wave increased. A waterfall spectrum constructed from high-speed pressure measurements taken during the run is shown in figure 10 and shows the switching between operation. Prior to 8 seconds the secondary wave is present in pressure measurements as a tone at approximately $1.1f_{CJ}$ with the main detonation wave appearing at approximately $0.8f_{CJ}$. However, past 8 seconds the secondary wave ceases to exist. At the same time the main detonation increases in speed by approximately 50 m/s or 3% of the ideal CJ detonation speed. A number of spectral tones present in the first half of the run also cease along with the counter wave pair. This suggests the tones were either direct representations of the wave or representations of the interaction between the main detonation wave and the secondary wave system. If wave speeds are taken to be a measure of the ideality of the detonation wave, then measurements suggest the presence of the counter propagating wave pair is in some form a non-ideality hindering the wave and impacting performance. Some of our ongoing work suggests a correlation between counter propagating waves and parasitic combustion in the fill region prior to the detonation wave where the impact of parasitic combustion reduces wave speed and pressure ratio when compared to the ideal case.[8,9]

VIII. Conclusions

The development of Circuit Wave Analysis has allowed for a greater understanding into the characteristics of wave systems present in rotating detonation engines. Over a wide range of operating conditions as well as air inlet and fuel injector configurations, the MRDE has been found to operate in some combination of three distinct wave systems: (1) the main detonation wave; (2) a counter-rotating fast wave; and (3) a

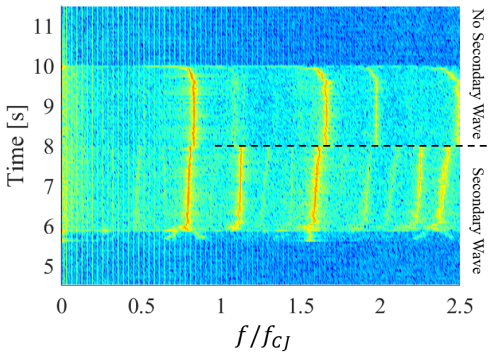

Figure 10. Waterfall spectrum constructed from high-speed pressure measurements for a single run. Halfway through the run the secondary wave system ceases to exist, correlating with an increase in detonation wave speed.

counter-rotating slow wave pair. The main detonation wave system is found for most operation conditions with secondary wave systems being present under specific operation conditions. The controlling mechanisms responsible for the secondary wave systems are not currently known and their prevalence at a given operation condition does not follow any easily discerned pattern. Some relationships between the various wave speeds have been identified, namely the matching of the counter propagating fast wave speed with the main detonation wave for most operation conditions. An additional potential dependence on equivalence ratio is observed in the relationship between detonation speed and counter propagating slow wave pair speed. A correlation between the presence of one of the counter propagating wave pair and the main detonation wave speed at constant operation conditions was observed, wherein the prevalence of the counter propagating wave pair correlated with a decrease in detonation speed. The mechanism by which the secondary wave system was creating a velocity deficit in the main detonation wave is not known, but is hypothesized to be related to parasitic combustion in the fill region as is observed in some of our concurrent studies.[8,9] The correlation implies that the secondary wave system poses a non-ideal hindrance to the detonation wave and may negatively impact performance.

References

[1]Bykovskii, F. A., Zhdan, S. A., and Vedernikov, E. F., "Continuous Spin Detonations," *Journal of Propulsion and Power*, Vol. 22, No. 6, nov 2006, pp. 1204–1216.

[2]Kindracki, J., Wolański, P., and Gut, Z., "Experimental research on the rotating detonation in gaseous fuels–oxygen mixtures," *Shock Waves*, Vol. 21, No. 2, jan 2011, pp. 75–84.

[3]Tellefsen, J., King, P., Schauer, F., and Hoke, J., "Analysis of an RDE with Convergent Nozzle in Preparation for Turbine Integration," *50th AIAA Aerospace Sciences Meeting including the New Horizons Forum and Aerospace Exposition*, American Institute of Aeronautics and Astronautics (AIAA), jan 2012.

[4]Driscoll, R., Anand, V., St George, A., and Gutmark, E., "Investigation on RDE operation by geometric variation of the combustor annulus and nozzle exit area," *9th US National Combustion Meeting*, 2015.

[5]Bluemner, R., Bohon, M., Paschereit, C. O., and Gutmark, E. J., "Dynamics of Counter-Rotating Wave Modes in an RDC," *2018 Joint Propulsion Conference*, American Institute of Aeronautics and Astronautics, jul 2018.

[6]Bohon, M., Bluemner, R., Paschereit, C., and Gutmark, E., "High-speed imaging of wave modes in an RDC," *Experimental Thermal and Fluid Science*, Vol. 102, apr 2019, pp. 28–37.

[7]Rankin, B. A., Richardson, D. R., Caswell, A. W., Naples, A. G., Hoke, J. L., and Schauer, F. R., "Chemiluminescence imaging of an optically accessible non-premixed rotating detonation engine," *Combustion and Flame*, Vol. 176, feb 2017, pp. 12–22.

[8]Chacon, F. and Gamba, M., "Study of Parasitic Combustion in an Optically Accessible Continuous Wave Rotating Detonation Engine," *Submitted to 2019 Scitech Meeting*, American Institute of Aeronautics and Astronautics, Jan 2019.

[9]Feleo, A., France, J., White, L., and Gamba, M., "Investigation of OH Chemiluminescence in Detonation Channel of a Rotating Detonation Engine," *Submitted to 2019 Scitech Meeting*, American Institute of Aeronautics and Astronautics, Jan 2019.

[10]Duvall, J., Chacon, F., Harvey, C., and Gamba, M., "Study of the Effects of Various Injection Geometries on the Operation of a Rotating Detonation Engine," *2018 AIAA Aerospace Sciences Meeting*, American Institute of Aeronautics and Astronautics, jan 2018.

[11]Schwer, D. and Kailasanath, K., "Feedback into Mixture Plenums in Rotating Detonation Engines," *50th AIAA Aerospace*

Sciences Meeting including the New Horizons Forum and Aerospace Exposition, American Institute of Aeronautics and Astronautics (AIAA), jan 2012.

[12]Gaillard, T., Davidenko, D., and Dupoirieux, F., "Numerical Optimisation in Non Reacting Conditions of the Injector Geometry for a Continuous Detonation Wave Rocket Engine," *Acta Astronautica*, Vol. 111, jun 2015, pp. 334–344.

[13]Chacon, F., Duvall, J., and Gamba, M., "Evaluation of Pressure Rise and Oscillation in a Rotating Detonation Engine," *2018 AIAA Aerospace Sciences Meeting*, American Institute of Aeronautics and Astronautics, jan 2018.

[14]Bennewitz, J. W., Bigler, B. R., Hargus, W. A., Danczyk, S. A., and Smith, R. D., "Characterization of Detonation Wave Propagation in a Rotating Detonation Rocket Engine using Direct High-Speed Imaging," *2018 Joint Propulsion Conference*, American Institute of Aeronautics and Astronautics, jul 2018.

Acknowledgments

This paper is based on work supported by the DOE/NETL University Turbine Systems Research under DOE DOE Grant No. FE0031228 with Robin Ames as program monitor.